THE JOURNAL OF PHYSICAL CHEMISTRY B

Article

pubs.acs.org/JPCB

Assigning Structures to Gas-Phase Peptide Cations and Cation-Radicals. An Infrared Multiphoton Dissociation, Ion Mobility, Electron Transfer, and Computational Study of a Histidine Peptide Ion

Christopher L. Moss,[†] Julia Chamot-Rooke,[‡] Edith Nicol,[‡] Jeffery Brown,[§] Iain Campuzano,[§,⊥] Keith Richardson,[§] Jonathan P. Williams,[§] Matthew F. Bush,[†] Benjamin Bythell,[∥,#] Bela Paizs,[∥] and Frantisek Turecek*[,†]

[†]Department of Chemistry, University of Washington, Bagley Hall, Box 351700, Seattle, Washington 981915-1700, United States

[‡]Laboratoire des Mécanismes Réactionnels, CNRS, École Polytechnique, Palaiseau, France

[§]Waters Corporation, Floats Road, Wythenshawe, Manchester, M23 9LZ, United Kingdom

[∥]German Cancer Research Center, Heidelberg, Germany

Supporting Information

ABSTRACT: Infrared multiphoton dissociation (IRMPD) spectroscopy, using a free-electron laser, and ion mobility measurements, using both drift-cell and traveling-wave instruments, were used to investigate the structure of gas-phase peptide $(AAHAL + 2H)^{2+}$ ions produced by electrospray ionization. The experimental data from the IRMPD spectra and collisional cross section (Ω) measurements were consistent with the respective infrared spectra and Ω calculated for the lowest-energy peptide ion conformer obtained by extensive molecular dynamics searches and combined density functional theory and *ab initio* geometry optimizations and energy calculations. Traveling-wave ion mobility measurements were employed to obtain the Ω of charge-reduced peptide cation-radicals, $(AAHAL + 2H)^{+\bullet}$, and the c_3, c_4, z_3, and z_4 fragments from electron-transfer dissociation (ETD) of $(AAHAL + 2H)^{2+}$. The experimental Ω for the ETD charge-reduced and fragment ions were consistent with the values calculated for fully optimized ion structures and indicated that the ions retained specific hydrogen bonding motifs from the precursor ion. In particular, the Ω for the doubly protonated ions and charge-reduced cation-radicals were nearly identical, indicating negligible unfolding and small secondary structure changes upon electron transfer. The experimental Ω for the $(AAHAL + 2H)^{+\bullet}$ cation-radicals were compatible with both zwitterionic and histidine radical structures formed by electron attachment to different sites in the precursor ion, but did not allow their distinction. The best agreement with the experimental Ω was found for ion structures fully optimized with M06-2X/6-31+G(d,p) and using both projection approximation and trajectory methods to calculate the theoretical Ω values.

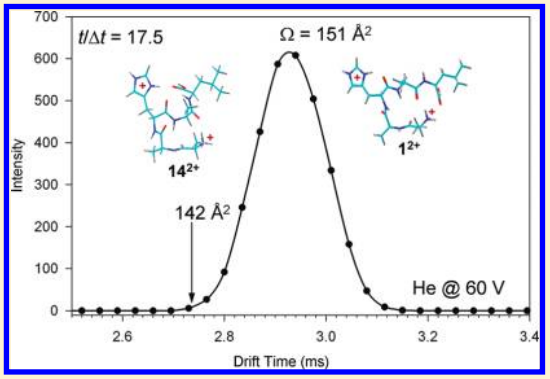

INTRODUCTION

Gas-phase ions that are produced and studied by mass spectrometry are transient species that often do not have structurally equivalent counterparts in the condensed phase. Hence, the methods of structure elucidation of gas-phase ions have some specifics that depend on the type of the ion of interest. Assigning structures to small organic gas-phase ions mainly relied on the combination of dissociation thermochemistry, dynamics, and product analysis[1] that was aided by electron structure theory calculations. With complex gas-phase ions such as those derived from peptides, detailed thermochemical and dynamic experiments are often unavailable. Furthermore, gas-phase peptide ions can exist as multiple tautomers differing in the protonation sites, and each tautomer can have multiple conformers that are not a priori known or predictable based on the peptide sequence. The experimental methods that are capable of assigning gas-phase peptide ion structures are infrared action spectroscopy[2−6] and ion mobility mass spectrometry (IMS),[7−10] both combined with molecular dynamics and electronic structure theory calculations that aid data interpretation. As these experimental methods have become more widely used, it has also become evident that they have inherent limitations. Infrared multiphoton dissociation (IRMPD) peak intensities sometimes do not correlate with the dipole strength of the corresponding vibrational excitations[11−14] and difficulties have been noticed with scaling the calculated vibrational frequencies. Strong hydrogen bonding leads to IRMPD bands that are difficult to assign to stretching vibrational modes.[15,16] IMS methods provide highly reproducible ion mobilities that are converted to collisional cross

Received: January 3, 2012
Revised: February 24, 2012
Published: February 27, 2012

sections (Ω) for the particular gas. However, matching the experimental Ω with calculated values is model dependent,[17−19] which limits the practically achievable accuracy to ca. ± 3%. Regarding computational structure analysis, MD calculations are unable to rank the tautomer energies and are unreliable in providing relative energies even for conformers of a given tautomer. Worse yet, electron structure computations that can handle medium-size (>50 atoms) peptide ions are limited to gradient optimizations using density functional theory (DFT) methods. The most popular DFT hybrid functional (B3LYP), in the form that implements the local exchange and correlation functional of Vosko et al.[20] and a nonlocal Lee−Yang−Parr functional with a gradient correction,[21] has a well-recognized deficiency in that it does not fully eliminate two-electron, four-center integrals involving the same electron in the exchange part of the functional, leading to what is known as the electron self-interaction error.[22−24] While this error is not critical in small molecular systems, it has been found to be quite serious for peptide ions of >150 atoms where B3LYP calculations showed convergence collapses.[25] These problems can possibly be overcome by compensating the energy errors inherent to B3LYP by perturbational (MP2) energy calculations.[26] MP2 calculations have been used to assign structures of small peptide ions.[27−33] However, MP2 scales with the fifth power of the number of electrons/atomic orbitals and becomes prohibitively expensive when the molecular size exceeds about 100 atoms, corresponding to a peptide ion of 6−7 amino acid residues. Some success has been achieved with DFT methods that mitigate or compensate the electron self-interaction, as in the Coulomb-attenuating version of B3LYP, CAM-B3LYP,[34] or the so-called universal functional M06-2X.[35,36]

We reasoned that it should be a combination of experimental and computational methods that would most likely provide reliable data regarding gas-phase peptide ion structures. Here, we report results from IRMPD, IMS, and computational methods to bear on the structure of gas-phase ions derived from doubly protonated pentapeptide AAHAL. This pentapeptide has been the subject of a previous study[37] aimed at what we call the histidine effect on electron transfer dissociations.[38−40] Thus, the gas-phase structures of both the precursor dication, its charge-reduced intermediates, and backbone dissociation products have been of interest to be addressed in detail here.

EXPERIMENTAL SECTION

IRMPD. The IRMPD spectra were measured using the CLIO free electron laser.[41] The experimental set up is based on a modified Bruker Esquire 3000 ion trap mass spectrometer. To allow the irradiation of the ions with the focused CLIO beam, a 0.7 mm hole was drilled in the ring electrode. The ions generated by an electrospray ion source are transferred to the trap by two octopoles. There, the ions are stabilized by collisions with the He bath gas at a pressure of 10^{-3} mbar. After a rapid thermalization, the ions are confined in a very small volume in the center of the trap. The laser beam was focused in the center of the trap using a 500 mm focal length ZnSe focal lens. The IR FEL CLIO light is delivered in 8 ms long macropulses fired at a repetition rate of 25 Hz. Each macropulse contains 500 micropulses, each a few picoseconds long. Following a 0.5 s relaxation time, the ions are mass selected and fragmented by macropulses of IR light. An electron energy of 45 MeV was used, which allowed access to wavelengths in the 1000−2000 cm^{-1} range.

The AAHAL peptide (GenScript, Piscataway, NJ) was electrosprayed from 10 μM solution in 50/50/1 methanol/water/acetic acid. The $(AAHAL + 2H)^{2+}$ ions at m/z 241.6 were stored in an ion trap and irradiated by IR photons from the free-electron laser for 250 or 500 ms. The main dissociation channels were monitored at m/z 218.5, 340, 411, 143, and 86, and the experimental IRMPD spectrum reported here was obtained considering all these fragmentation channels. The reported experimental IRMPD spectrum is a sum of two measurements and plots the fragmentation efficiency, defined as $-\ln\{[parent]/([parent] + [fragments])\}$ where square brackets indicate parent and fragment ion intensities, as a function of the photon wavenumber. A linear correction of the IRMPD yield with the laser power was carried out.[41] The spectrum was smoothed using a three-point running average fit.

Ion Mobility. The absolute mobility (K) of $(AAHAL + 2H)^{2+}$ in helium was measured using a modified Synapt G1 HDMS (Waters Co., Manchester, U.K.) instrument in which the traveling-wave ion mobility cell was replaced with an 18-cm drift cell that has radial RF ion confinement and a linear voltage gradient to direct ions along the axis of transmission to the time-of-flight mass analyzer. This cell uses no traveling waves, and is discussed in detail elsewhere.[42] K was determined from the slope of a drift time versus reciprocal drift voltage plot (R^2 = 0.999997, Figure S1, Supporting Information) containing measurements at ten drift voltages ranging from 60−200 V in 2.500 Torr of helium gas at 301 K. The collision cross section in helium for $(AAHAL + 2H)^{2+}$ was determined using that K and the Mason-Schamp equation.[43] Although the relative error for that measurement is very small (<0.1%), the absolute error is estimated to be 2−3%.

Another set of ion mobility measurements was carried out in a T-wave ion mobility cell of a hybrid quadrupole/ion mobility/orthogonal-acceleration time-of-flight (ToF) mass spectrometer fitted with electron transfer dissociation capability (Synapt-G2 HDMS, Waters, U.K.). The instrument is described in detail elsewhere.[44−46] Briefly, the instrument incorporates a series of three T-Wave cells prior to the ToF mass analyzer. For ETD-IMS studies, a subambient pressure (2 mbar) glow discharge anion source repetitively fills the first cell (Trap T-Wave cell) with quadrupole mass selected ETD reagent anions (1,3-dicyanobenzene m/z 128). The AAHAL peptide was prepared at a concentration of 1 μM in 50/50 acetonitrile/water with 0.1% formic acid. Peptides were infused into the nano-electrospray source at a flow rate of 300 nL/min. The quadrupole mass-selected $(AAHAL + 2H)^{2+}$ ions were flown through the previously stored reagent anions in the Trap T-Wave. The resulting ion−ion reaction products were subsequently separated according to their ion mobilities in the second cell (IMS T-Wave cell). A third cell (transfer cell) was used to transfer ions into the ToF (or provide an optional stage of supplemental (CID)). The ToF detection system recorded both the time-of-flight of the product ions in addition to the ion mobility drift times. In this study, the T-Wave of the IMS cell was set with a wave amplitude of 25 V and a wave speed of 650 m/s. The IMS cell was pressurized with 2.5 mbar of N_2.

Collisional cross sections (Ω) were derived using the ion mobility calibration and visualization software. (Driftscope v2.2 Waters). For singly charged ions, known Ω reference values[47] for polyalanine were used to generate a T-Wave calibration function relating drift time to the Ω. In order to derive the Ω for the doubly charged $(AAHAL + 2H)^{2+}$ ions, a mixture of

Table 1. Relative Energies of $(AAHAL + 2H)^{2+}$ Ions

		relative energy[a,b]						
ion	type	B3LYP 6-31+G(d,p)	B3LYP 6-311++G(2d,p)	MP2[c]	B3-MP2[d]	CAM-B3LYP[c] 6-311++G(2d,p)	M06-2X[e] 6-311++G(2d,p)	ωB97x[c]
1^{2+}	A	0	0	0	0 (0.0)[f]	0	0	0
2^{2+}	A	6	6	6	6 (7)[f]	6	6	5
3^{2+}	A	7	7	16	11 (8)[f]	8	12	11
4^{2+}	B	9	11	−4	4 (15)[f]	6	4	1
5^{2+}	B	10	12	−7	3 (14)[f]	7	3	7
6^{2+}	A	10	10	20	15 (18)[f]	12	14	14
7^{2+}	B	13	14	−2	6 (19)[f]	9	5	3
8^{2+}	A	13	13	12	13 (13)[f]	11	13	14
9^{2+}	AB	13	13	16	15 (21)[f]	–	–	–
10^{2+}	A	13	13	17	15 (18)[f]	–	–	–
11^{2+}	B	14	16	−3	7 (20)[f]	11	5	3
12^{2+}	A	14	14	11	13 (15)[f]	–	–	–
13^{2+}	AB	14	14	14	14 (19)[f]	–	–	–
14^{2+}	C	14	14	−6	4 (13)[f]	10	3	5
15^{2+}	AB	17	20	−1	9 (22)[f]	13	7	5
16^{2+}	AB	17	18	2	10 (24)[f]	13	8	6
17^{2+}	C	20	21	−2	9 (22)[f]	16	7	9

[a]In units of kJ mol^{-1}. [b]Including B3LYP/6-31+G(d,p) zero-point energies and referring to 0 K. [c]From single-point energies with the 6-311++G(2d,p) basis set on B3LYP/6-31+G(d,p) optimized geometries. [d]From averaged B3LYP and MP2/6-311++G(2d,p) single point energies. [e]From single-point energies on M06-2X/6-31+G(d,p) optimized geometries. [f]Relative free energies at 298 K.

doubly charged reference peptide ions Ser-Asp-Gly-Arg-Gly and Gly-Arg-Gly-Asp-Ser were analyzed and the drift time of the $(AAHAL + 2H)^{2+}$ lay between the two reference species. Previous DC drift tube studies[48] reported Ω in helium for doubly protonated SDGRG and GRGDS peptide ions as 145.6 and 149.7 $Å^2$, respectively.

Calculations. Two conformational search engines were employed to provide an initial list of ion structures. Since the AAHAL peptide contains basic groups at the His imidazole ring and at the N-terminal amino group, only tautomers protonated at these positions were considered. The first search engine[49] used molecular dynamics (MD) simulations using the Insight II program (Biosym Technologies, San Diego, CA) and a modified AMBER force field.[50] The structures generated in the MD run were annealed to generate 1050 nonidentical conformers that were optimized by PM3 and ranked by single-point energies obtained with HF/3-21G. The resulting structures were analyzed by a conformer family search to eliminate duplicates, which provided 993 structures in 307 families. A total of 49 lowest-energy conformers were reoptimized with HF/3-21G calculations, and the resulting structures were again sorted out to give 44 nondegenerate structures in 20 families. Thirty lowest-energy structures of this reduced set were optimized with B3LYP/6-31+G(d,p) and the resulting conformers were again sorted out to yield 28 nondegenerate structures. The electronic structure calculations used the Gaussian 03 suite of programs.[51]

The other search engine[52] started with molecular dynamics calculations using NAMD[53] and parameters from the CHARMM force field.[54] Replica exchange molecular dynamics (REMD)[55] calculations were performed which were run for 10 ns with a step size of 1 fs over 8 temperature replicas from 300 to 800 K. One thousand structures from each temperature replica were stored for a total of 8000 structures and fully reoptimized with PM6.[56] The PM6 optimized structures were then sorted out by their hydrogen bond patterns into families. The lowest-energy structure in each family was treated with single-point B3LYP/6-31+G(d,p) calculations,[57−59] which provided a more reliable energy ranking to select conformers for final geometry optimizations and higher-level energy calculations.

Forty two lowest-energy structures from the list generated by the REMD/PM6/B3LYP search engine were then reoptimized with B3LYP/6-31+G(d,p) and confirmed as local energy minima by frequency analysis. The calculated harmonic frequencies were scaled by 0.986 to provide the closest match with the bands in the IRMPD spectra. For comparison with IRMPD data, the calculated IR bands were convoluted with Lorentzian function profiles broadened to 20 cm^{-1} full width at half-maximum (fwhm). Single point energies were calculated on 70 B3LYP/6-31+G(d,p) optimized structures that were combined from the above-described conformational searches, using the B3LYP, CAM-B3LYP,[34] and ωB97x[60] functionals and the 6-311++G(2d,p) basis set. Another set of single-point energies were obtained with Møller−Plesset (MP2, frozen core) calculations[61] and the 6-311++G(2d,p) basis set, and the MP2 and B3LYP energies were averaged (B3-MP2) to cancel errors inherent to each method.[26] Several low-energy structures selected from the combined B3-MP2 single-point energy calculations were reoptimized with the M06-2X functional[35] and the 6-31+G(d,p) basis set, and the reoptimized structures were used for single-point energy M06-2X/6-311++G(2d,p) calculations. These electronic structure calculations used the Gaussian 09 suite of programs.[62] Wave numbers and infrared band intensities were obtained for ion structures that were fully optimized with both B3LYP/6-31+G(d,p) and M06-2X/6-31+G(d,p).

Theoretical Collision Cross-Section Calculations. Gaussian output files were batch converted into pdb files and mfj[63] files for projection approximation (PA)[64,65] and trajectory method (TM)[66] calculations, respectively. Charges obtained from natural population analysis[67] with M06-2X or B3LYP/6-311++G(2d,p) were included in the mfj files to allow calculation of dipole interactions between the analyte and the polarizable drift gas molecules. PA calculations were performed using the implementation in Waters' DriftScope software. The

dx.doi.org/10.1021/jp3000784 | J. Phys. Chem. B 2012, 116, 3445−3456

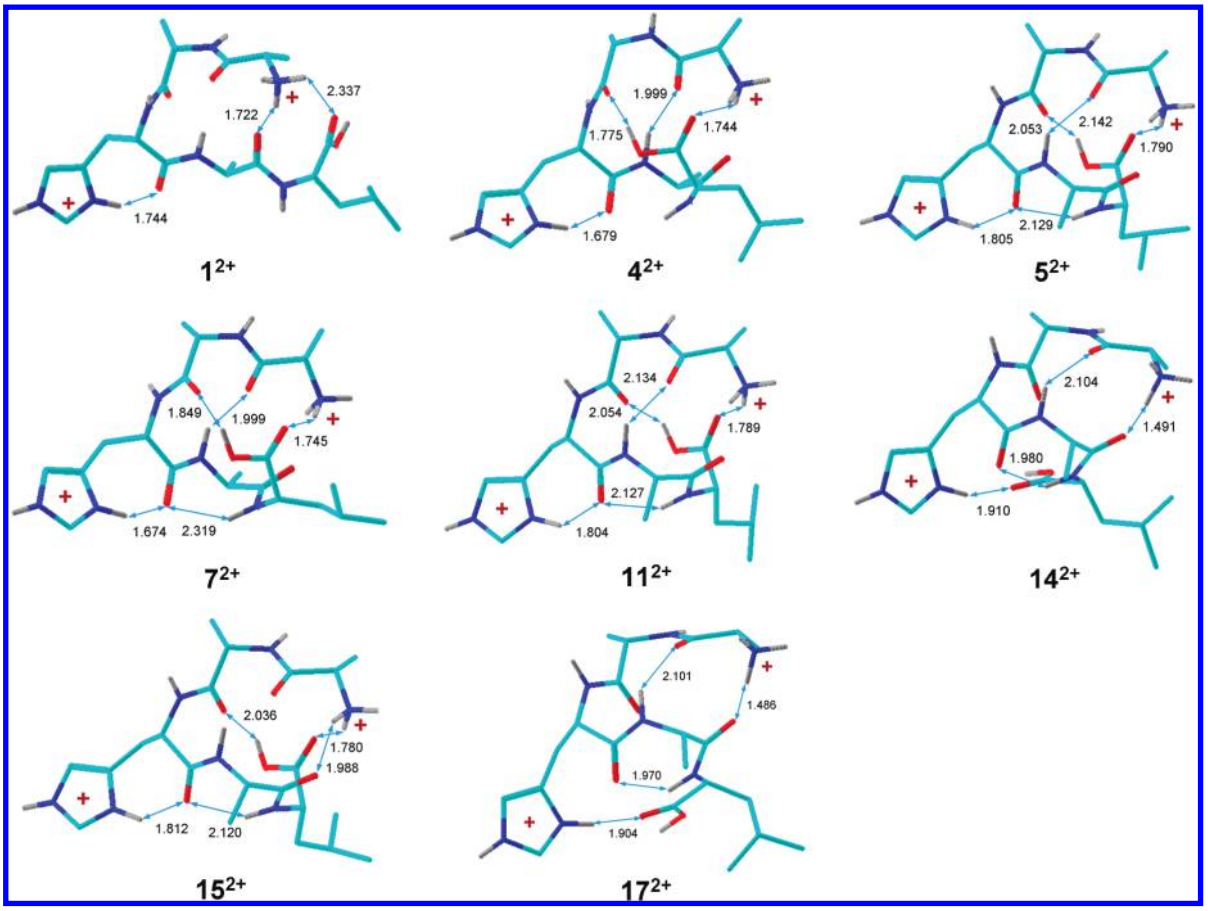

Figure 1. Representative M06-2X optimized ion structures. The atoms are color-coded as follows: green = C, blue = N, red = O, and gray = H. Only exchangeable (OH, NH) hydrogen atoms are shown. Hydrogen bonds are denoted by blue double-ended arrows. The H-bond lengths are given in Ångstrøms.

hard-sphere radii employed were identical to those used in the freely available version of the Mobcal software. Theoretical helium collision cross sections (Ω_{He}) were calculated using a modified trajectory method algorithm.[68,69] Briefly, the trajectory method[66] was originally developed by Jarrold and co-workers to calculate the theoretical Ω of an ion based on its interaction with the IM buffer gas helium. The potential term utilized in the trajectory method is based on the two-body 12−6 potential model representing the sum of a two-body (ion-neutral), short-range, van der Waals interactions and also incorporating a long-range, ion-induced dipole, attractive interaction which incorporates the polarizability of the drift gas, in this case helium. It was felt that the trajectory method was the most appropriate algorithm to use for this study since the ion species being investigated were a mixture of doubly charged even electron ions and odd electron radical cations, and an algorithm, which can take into account accurately derived ionic surface charges, thus accurately describing the long-range potential effect of the ion mobility separation, was highly desirable. Since single, quantum-theory optimized, structures are being processed, the impact factor, that is, the number of points within the Monte Carlo integration of the impact and orientation, of the trajectory method was increased from the default value of 25 to 1000, resulting in a total number of 400 000 sampling points and a dramatically improved standard deviation value (≤1.3%). The modified trajectory method was implemented on a LINUX based HP Z600 12 processor workstation.

RESULTS AND DISCUSSION

We first present and discuss the ion structures and relative energies obtained by the computational methods employed here. The ion structure and spectroscopic properties are then compared with experimental data obtained by IMS and IRMPD measurements. Geometry optimizations were carried out for 70 ion structures that were then ranked by their single-point energies from combined B3LYP and MP2/6-311++G(2d,p) calculations (B3-MP2). The relative energies for 17 lowest-energy structures are given in Table 1, and selected structures are shown in Figure 1. Cartesian coordinates for optimized ion structures $\mathbf{1}^{2+}$−$\mathbf{17}^{2+}$ are given in Tables S1−S25 (Supporting Information). The conspicuous feature of the Table 1 data is that the relative energy rankings by B3LYP and MP2 dramatically differ. The ion structures fall into four groups that differ in their hydrogen bonding patterns. Group A consists of conformers $\mathbf{1}^{2+}$−$\mathbf{3}^{2+}$, $\mathbf{6}^{2+}$, $\mathbf{8}^{2+}$, $\mathbf{10}^{2+}$, and $\mathbf{12}^{2+}$ which have the protonated His group H-bonded to the His amide carbonyl, and the N-terminal NH_3 group is H-bonded to the Ala-4 amide carbonyl. Group A is represented by the most stable conformer $\mathbf{1}^{2+}$ (Figure 1). Group B consists of conformers $\mathbf{4}^{2+}$, $\mathbf{5}^{2+}$, $\mathbf{7}^{2+}$, and $\mathbf{11}^{2+}$. These conformers have the protonated His group H-bonded to the His amide carbonyl, and the N-terminal NH_3 group is H-bonded to the COOH group. Note that Group B conformers are preferred by MP2 calculations that place ion $\mathbf{5}^{2+}$ as the lowest-energy structure (Figure 1). The next group (AB) consists of ion conformers $\mathbf{9}^{2+}$, $\mathbf{13}^{2+}$, $\mathbf{15}^{2+}$, and $\mathbf{16}^{2+}$, which have the protonated His group H-bonded to the His amide carbonyl,

dx.doi.org/10.1021/jp3000784 | J. Phys. Chem. B 2012, 116, 3445−3456

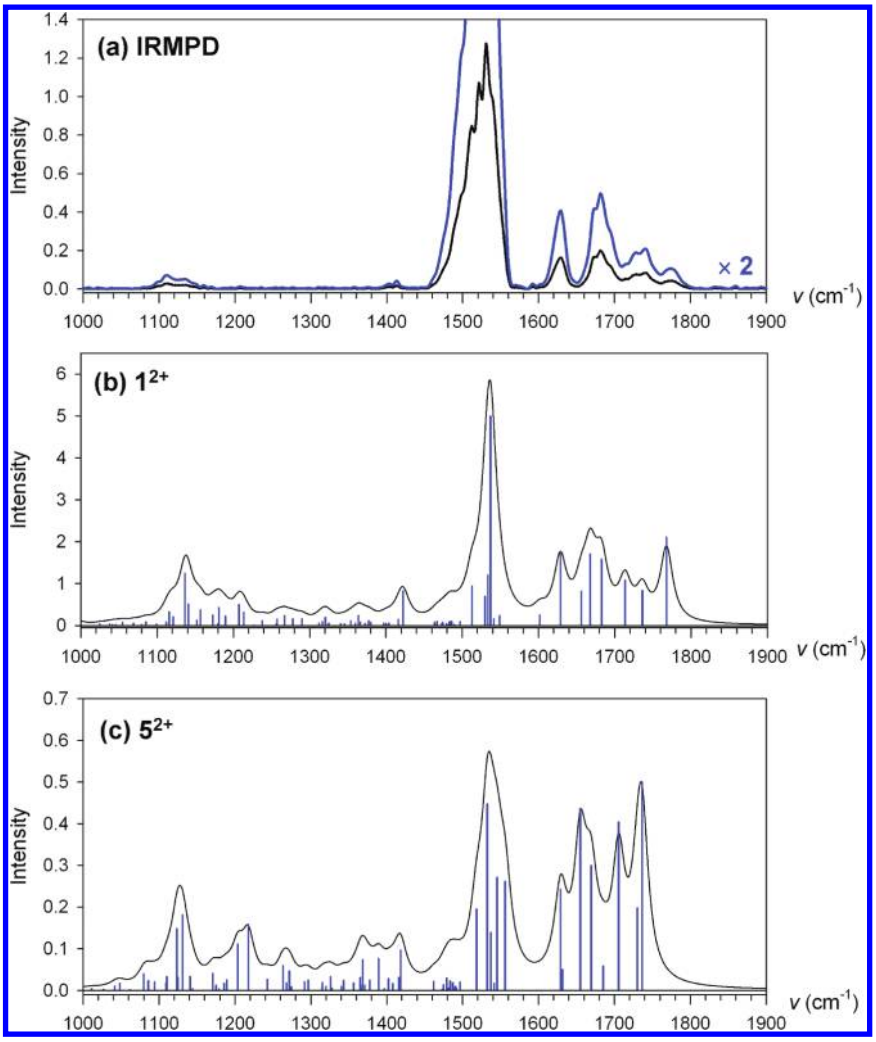

Figure 2. (a) IRMPD of $(AAHAL + 2H)^{2+}$ and calculated IR spectra of (b) $\mathbf{1}^{2+}$ and (c) $\mathbf{5}^{2+}$. The bands in the calculated spectra were broadened with Lorenzian functions to 20 cm^{-1} fwhm.

and the N-terminal NH_3 group is H-bonded to both the Ala-4 amide carbonyl and the COOH group. The most stable conformer of group AB ($\mathbf{15}^{2+}$, Figure 1) is disfavored by B3LYP, but favored by MP2. Finally, group C consist of conformers $\mathbf{14}^{2+}$ and $\mathbf{17}^{2+}$, which have the protonated His group H-bonded to the COOH group, and the N-terminal NH_3 group is H-bonded to the Ala-4 amide carbonyl (Figure 1). Group C conformers are disfavored by B3LYP but favored by MP2. We note that all the other conformers for which we obtained optimized structures and single-point energies were disfavored against $\mathbf{1}^{2+}$–$\mathbf{17}^{2+}$ by both B3LYP and MP2 calculations and were presumably less stable than the set shown in Table 1.

The difference between the B3LYP and MP2 energy rankings is of concern, because if only one type of calculations was used they would result in different structure assignments. An empirical correction to B3LYP and MP2 results has been proposed and used previously that was based on averaging the single-point energies. This provided improved relative energies for several systems.[26,37−39] However, the empirical nature of this correction is of concern, especially if the B3LYP and MP2 relative energies diverge by more than is the typical confidence interval of relative energies for each method (ca. 20 kJ mol^{-1}). The differences between the B3LYP and MP2 relative energies for groups A−C ions appear to be linked to the degree of intramolecular hydrogen bonding. In particular, group B and C ions exhibit a larger number of hydrogen bonds, involving both the neutral and ionic groups and resulting in more compact structures compared to group A and AB structures. This can be expressed through the electron spatial extent[70] which is the expectation value of the square of the electron coordinate vector, $\langle \psi_{el} | r_{el}^2 | \psi_{el} \rangle$, which correlates with the molecular volume.[71] The electron spatial extent calculated with B3LYP/6-311++G(2d,p) was 20−25% smaller for $\mathbf{4}^{2+}$, $\mathbf{5}^{2+}$, $\mathbf{7}^{2+}$, $\mathbf{11}^{2+}$, and $\mathbf{14}^{2+}$ (4403−4699 $Å^2$) compared to $\mathbf{1}^{2+}$ (5893 $Å^2$) This increased compactness affects the electron density and may have an effect on both the electron correlation energy, which is recovered incompletely (~85−90%) by MP2,[72,73] and the self-electron interaction in the exchange-correlation functional which is not completely compensated in B3LYP.[22−24]

To investigate the latter effect, we obtained single point energies by DFT methods that mitigate or reduce self-electron interaction. The Coulomb-attenuating B3LYP (CAM-B3LYP),[34] ωB97x,[60] and M06-2X[35] density functionals were used to calculate single point-energies for a subset of ions in Table 1. The presented CAM-B3LYP and ωB97x/6-311++G(2d,p) single-point energies were run on B3LYP-optimized geometries. The M06-2X/6-311++G(2d,p) single-point ener-

dx.doi.org/10.1021/jp3000784 | J. Phys. Chem. B 2012, 116, 3445−3456

gies were run on both B3LYP geometries and those that were fully optimized with M06-2X/6-31+G(d,p). Table 1 data show that both the ωB97x and M06-2X relative energies are very close to those from averaged B3LYP and MP2 calculations, the root-mean-square deviations (rmsd) being 2.4 and 1.5 kJ mol^{-1}, respectively. The fit with B3-MP2 of the CAM-B3LYP relative energies was somewhat less tight, but still acceptable with an rmsd of 3.7 kJ mol^{-1}. Note that CAM-B3LYP, ωB97x, and M06-2X all identified $\mathbf{1}^{2+}$ as the lowest-energy conformer in complete agreement with B3-MP2.

As discussed below, the optimized M06-2X/6-31+G(d,p) geometries showed small but systematic differences from the B3LYP/6-31+G(d,p) ones. This resulted in total single-point energies obtained by M06-2X/6-311++G(2d,p) being 6.9−8.7 millihartree higher when using B3LYP-optimized geometries for $\mathbf{1}^{2+}$-$\mathbf{17}^{2+}$. These energy differences (18−23 kJ mol^{-1}) can alter the energy ranking of the ion conformers, and so the use of fully optimized M06-2X/6-31+G(d,p) geometries for single-point calculations is to be preferred.

The conformer structures have a pronounced effect on the relative entropies that affect the ion relative free energies. The compact structures of groups B and C have substantially lower entropies than the group A and group AB structures. This is mainly due to vibrational entropy terms where the less compact A and AB structures display lower-frequency skeletal deformation modes than do the tighter B and C group structures. The synergistic enthalpy and entropy effects favor group A structures in general and conformer $\mathbf{1}^{2+}$ in particular. Thus, according to B3-MP2, CAM-B3LYP, ωB97x, and M06-2X, ion $\mathbf{1}^{2+}$ was calculated to constitute 89, 82, 86, and 91%, respectively, of an equilibrium mixture at 298 K, with Leu side-chain rotamers $\mathbf{2}^{2+}$ and $\mathbf{3}^{2+}$ contributing 8−9%. We conclude that according to electronic structure calculations, the equilibrium population of (AAHAL + 2H)$^{2+}$ ions should be dominated by Group A structures.

IRMPD Spectra. The experimental IRMPD spectrum of (AAHAL +2H)$^{2+}$ ions produced by electrospray and stored in a quadrupole ion trap is shown in Figure 2a. The IRMPD data were acquired at 250 and 500 ms irradiation time which gave identical spectra. This indicated that kinetic effects on IRMPD were negligible.[11] The spectrum shows strong overlapping bands in the 1500−1540 cm^{-1} region. Vibrational analysis of the calculated IR spectra of representative ion structures $\mathbf{1}^{2+}$ and $\mathbf{5}^{2+}$ (Figure 2b,c) showed that the 1500−1540 cm^{-1} absorption is due to amide II bands of transitions involving in-plane N−H bending vibrations of the four amide groups.[74] These appear at very similar wave numbers in several ion conformers and thus are not diagnostically useful. The diagnostically most valuable bands appear in the region of 1600−1800 cm^{-1}. The IRMPD spectrum shows six bands in this region, appearing at 1772, 1742, 1728, 1690, 1675, and 1628 cm^{-1} (Figure 3). These closely match the absorption bands of $\mathbf{1}^{2+}$ calculated by B3LYP that appear at 1768, 1736, 1713, 1682, 1668, and 1629 cm^{-1}. Vibrational analysis assigns the 1768 cm^{-1} band from $\mathbf{1}^{2+}$ to the stretching vibration of the carboxyl C═O. The 1736 and 1713 cm^{-1} bands belong to the Ala-2 and Ala-1 amide C═O stretching modes. Note that these amide groups do not have strong hydrogen-bonds to the protonated N-terminal or imidazole groups. The 1682 and 1668 cm^{-1} bands belong to combinations of His and Ala-4 amide C═O stretching modes and the imidazole N−H in-plane bending mode. These amide groups are engaged in hydrogen bonding to the protons of the charged groups (Figure 1). The 1629 cm^{-1} band belongs to the imidazole ring stretch involving mainly the C═C bond. The IR spectra in Figure 3 further show that low-energy representatives of the conformer groups B and C ($\mathbf{5}^{2+}$ and $\mathbf{14}^{2+}$, respectively) have different patterns of the C═O stretching bands. In particular, the spectra of $\mathbf{5}^{2+}$, and $\mathbf{14}^{2+}$ lack the high frequency band of the C═O stretch of the free carboxyl group, which is typical of $\mathbf{1}^{2+}$ and appears in the experimental IRMPD spectrum. This lack is consistent with the calculated structures of the group B and C ions, which all have the COOH group hydrogen-bonded to protons of one of the charged groups. Distinction by IRMPD spectra is less definite among the conformers belonging to group A that differ only in the conformation of the Leu side chain, which does not give rise to strong absorption bands in the 1000−1900 cm^{-1} region. However, the calculated relative energies and free energies unambiguously point to $\mathbf{1}^{2+}$ as the thermodynamically most stable structure, and thus we assign the experimental IRMPD spectrum to this conformer.

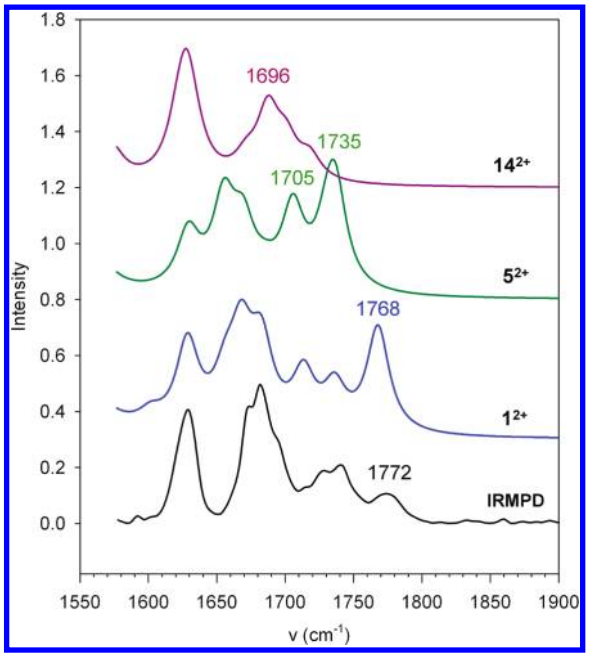

Figure 3. IRMPD and calculated IR spectra of $\mathbf{1}^{2+}$, $\mathbf{5}^{2+}$, and $\mathbf{14}^{2+}$ showing the 1550−1900 cm^{-1} region. The bands in the calculated spectra were broadened to 20 cm^{-1} fwhm.

IR spectra of the low-energy conformers $\mathbf{1}^{2+}$ (group A), $\mathbf{4}^{2+}$ and $\mathbf{5}^{2+}$ (group B), and $\mathbf{14}^{2+}$ (group C) were also calculated with M06-2X/6-31+G(d,p) (Figures S2 and S3, Supporting Information). The M06-2X IR spectra of $\mathbf{1}^{2+}$ and its Leu side-chain rotamer $\mathbf{2}^{2+}$ show the best match with the experimental IRMPD spectrum regarding the wave numbers (1768, 1732, 1694, 1675, 1650, 1612 cm^{-1}) and absorption intensities. Note that the M06-2X IR spectra of $\mathbf{4}^{2+}$, $\mathbf{5}^{2+}$, and $\mathbf{14}^{2+}$ (Figure S3, Supporting Information) show much greater variations of the calculated absorption intensities of the amide I and amide II bands than do the corresponding B3LYP IR spectra in Figures 2 and 3. The nature of these variations is currently unknown, but could be of concern if M06-2X IR spectra were used for assignment.

Ion Mobility. Ion mobility of (AAHAL + 2H)$^{2+}$ ions produced by electrospray was studied in both drift cell[42] and traveling wave modes[44−46] using helium and nitrogen as bath gases. The arrival time distributions and collisional cross sections (Ω) are shown in Figure 4. In each measurement, the

dx.doi.org/10.1021/jp3000784 | J. Phys. Chem. B 2012, 116, 3445−3456

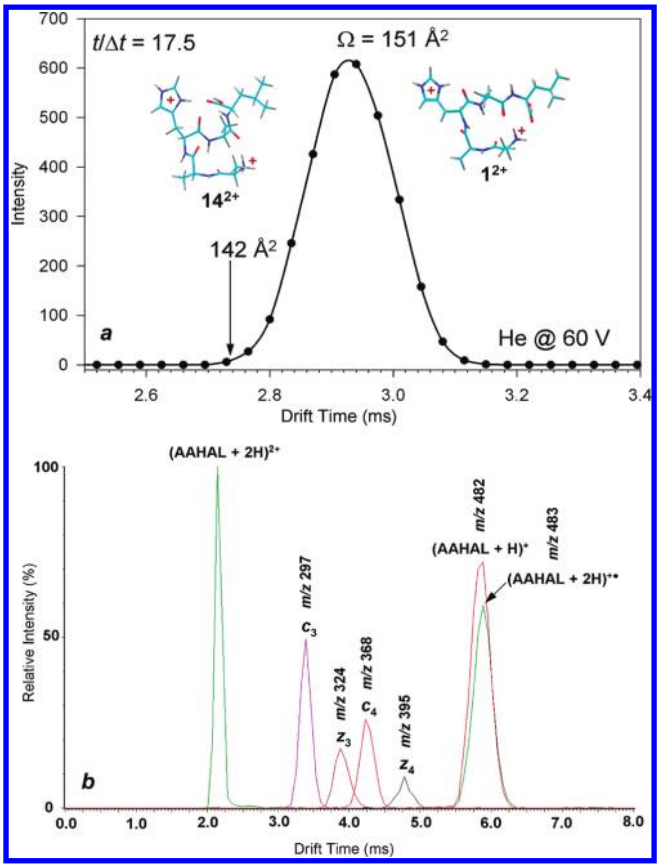

Figure 4. Ion mobility spectra. Top panel: $(AAHAL + 2H)^{2+}$ from drift-cell measurements. Bottom panel: $(AAHAL + 2H)^{2+}$ and ETD products from TWAVE measurements.

ion mobility showed a single peak for the $(AAHAL + 2H)^{2+}$ ion. The Ω in helium were calculated as 147 and 151 Å^2 for the TWave and drift cell measurements, respectively. The experimental Ω are now compared with the calculated values using the projection approximation (PA)[64,65] and trajectory method (TM)[66] models of converting the optimized ion geometries and charge distributions to collisional cross sections (Table 2). The Ω calculated with PA were 1.3−4% smaller than those calculated with TM. In addition, the M06-2X optimized structures gave Ω values that were 2−3.5% smaller than those based on B3LYP-optimized structures. Given the range of the calculated Ω, all structures in Table 2 would be compatible with the 147−151 Å^2 range of experimental cross sections. However, Figure 4a shows that ions with Ω differing by 10 Å^2 would be resolved in the drift cell measurements. For example, if structures $\mathbf{1}^{2+}$ and $\mathbf{14}^{2+}$ were present, they would appear as two separate ion mobility peaks, which was not observed. Thus, the ion mobility measurements are compatible with the presence of one dominant conformer of $(AAHAL + 2H)^{2+}$ ions formed by electrospray. However, ion mobility data alone would not allow structure assignment on the basis of collisional cross sections in this case.

Table 2. Collisional Cross Sections of $(AAHAL + 2H)^{2+}$ Ions

	cross section (Ω, Å^2)[a]			
	projection average		trajectory method	
ion	B3LYP	M06-2X	B3LYP	M06-2X
$\mathbf{1}^{2+}$	156	152	158	153
$\mathbf{4}^{2+}$	149	146	153	150
$\mathbf{5}^{2+}$	148	146	153	150
$\mathbf{7}^{2+}$	149	145	153	150
$\mathbf{11}^{2+}$	148	145	152	150
$\mathbf{14}^{2+}$	147	142	153	147

[a]The experimental Ω were 147 and 151 Å^2 from the TWAVE and drift-cell measurements, respectively.

Structures and Ion Mobility of Products of Electron Transfer. Whereas structure analysis of even-electron gas-phase peptide ions can be achieved by a combination of ion spectroscopy and electronic structure calculations, the situation is more difficult as concerns reactive intermediates or fragments produced by electron capture or transfer. Up to date, only a single assignment has been claimed by IRMPD for a small *c* fragment ion in an electron capture dissociation mass spectrum.[75] We utilized the capability of the Synapt G2 instrument to perform ion mobility measurements on the products of electron transfer to gas-phase peptide ions.[76] Figure 4b shows the arrival times of products of electron transfer to $(AAHAL + 2H)^{2+}$. Electron transfer to histidine-containing peptide ions is known to form stable charge-reduced cation-radicals (the histidine effect).[37−40] The peak for $(AAHAL + 2H)^{+\bullet}$ (m/z 483) contained ~30% of the ^{13}C isotopologue of $(AAHAL + H)^+$ (m/z 482) in the ETD mass spectrum. Both ions appeared at nearly identical arrival times and were assigned the Ω of 148−149 Å^2 (Figure 4b) Rather unexpectedly, the Ω of the charge-reduced $(AAHAL + 2H)^{+\bullet}$ and $(AAHAL + H)^+$ ions were quite similar to that of the $(AAHAL + 2H)^{2+}$ precursor ion. Structure assignment for $(AAHAL + 2H)^{+\bullet}$ was attempted by comparing the experimental Ω of the charge-reduced ion with those calculated for several cation-radical structure candidates.

Electron attachment to $(AAHAL + 2H)^{2+}$ presumably gives rise to an initial $(AAHAL + 2H)^{+\bullet}$ structure which then can undergo conformational reorganization and exothermic proton transfers to form various tautomers and conformers.[37] The driving force for such isomerizations is provided by the decrease of free energy. However, whether or not an isomerization occurs on the time scale of the experiment depends on the pertinent transition state energy[37] and the internal energy of the cation-radical. The relative enthalpies for the $(AAHAL + 2H)^{+\bullet}$ cation-radicals are given in Table 3. Electron attachment to ion $\mathbf{1}^{2+}$ gives two initial structures ($\mathbf{1a}^{+\bullet}$ and $\mathbf{1b}^{+\bullet}$) which are local energy minima (Figure 5). The more stable structure $\mathbf{1a}^{+\bullet}$ is an aminoketyl zwitterion by both B3LYP and M06-2X calculations. The other structure ($\mathbf{1b}^{+\bullet}$) is a classical His imidazolium radical.[39,40,77] The Ω calculated for $\mathbf{1a}^{+\bullet}$ and $\mathbf{1b}^{+\bullet}$ are well within the 3% error limits of the PA and TM models and must be considered indistinguishable by ion mobility. Note that the Ω that were based on the M06-2X-optimized structures showed a nearly perfect match with the experimental values, although the Ω from the B3LYP calculations were also within the combined error limits of the experimental measurements and Ω calculations. Peptide backbone rotation in $\mathbf{1a}^{+\bullet}$ leads to structure $\mathbf{2a}^{+\bullet}$ which is practically isoenergetic with and slightly more compact than $\mathbf{1a}^{+\bullet}$, as judged by its smaller Ω. Likewise, backbone rotation in $\mathbf{1b}^{+\bullet}$ leads to more stable conformers $\mathbf{2b}^{+\bullet}$ and $\mathbf{3b}^{+\bullet}$ which have smaller Ω than that of $\mathbf{1b}^{+\bullet}$ when based on the PA model, but not when assessed by the TM model. A more dramatic transformation by proton migration in $\mathbf{1b}^{+\bullet}$-$\mathbf{3b}^{+\bullet}$ can form imidazoline cation-radicals $\mathbf{4a}^{+\bullet}$ and $\mathbf{4b}^{+\bullet}$ (Figure 5). These

dx.doi.org/10.1021/jp3000784 | J. Phys. Chem. B 2012, 116, 3445−3456

Table 3. Relative Energies of (AAHAL + 2H)$^{+\bullet}$ Cation Radicals

	relative energy[a,b]				
	6-31+G(d,p)	6-311++G(2d,p)			
ion	B3LYP	B3LYP	MP2[c]	B3-MP2[d]	M06-2X[e]
1a$^{+\bullet}$	0	0	0	0	0
1b$^{+\bullet}$	5	0	16	8	13
2a$^{+\bullet}$	4	5	−14	−4	−3
2b$^{+\bullet}$	−16	−19	−24	−22	−18
3b$^{+\bullet}$	−17	−19	−23	−21	−17
4a$^{+\bullet}$	−90	−93	−87	−90	−83
4b$^{+\bullet}$	−107	−113	−82	−97	−85

[a]In units of kJ mol^{-1}. [b]Including B3LYP/6-31+G(d,p) zero-point energies and referring to 0 K. [c]From single-point energies with the 6-311++G(2d,p) basis set on B3LYP/6-31+G(d,p) optimized geometries. [d]From averaged B3LYP and MP2/6-311++G(2d,p) single point energies. [e]From single-point energies on M06-2X/6-31+G(d,p) optimized geometries.

are substantially more stable than **1a**$^{+\bullet}$ and **1b**$^{+\bullet}$ and are expected to dominate if the nondissociating cation-radicals were at equilibrium. The calculated Ω of **4a**$^{+\bullet}$ and **4b**$^{+\bullet}$ again depend on the employed model. Structure **4a**$^{+\bullet}$ is more compact than **1a**$^{+\bullet}$ when based on the PA Ω, but only marginally so when based on the TM Ω. Structure **4b**$^{+\bullet}$ is more spatially extended as shown by both PA and TM Ω, which showed the worst match with the experimental value. It should be noted that we did not consider in our analysis the several proper aminoketyl isomers[78] of **1a**$^{+\bullet}$**−3b**$^{+\bullet}$ and ion−molecule complexes reported previously,[37] because those would presumably dissociate on the time scale of the measurements.

In spite of the fact that detailed structure assignment of tautomers and conformers was difficult to achieve for the charge-reduced ions on the basis of their Ω, the experiment and theory showed a remarkable agreement. In particular, the measured Ω showed that charge-reduction did not result in any substantial refolding of the peptide ion, as several of the low-energy structures calculated for the cation-radical conformers and tautomers had the Ω close to the experimental value. This

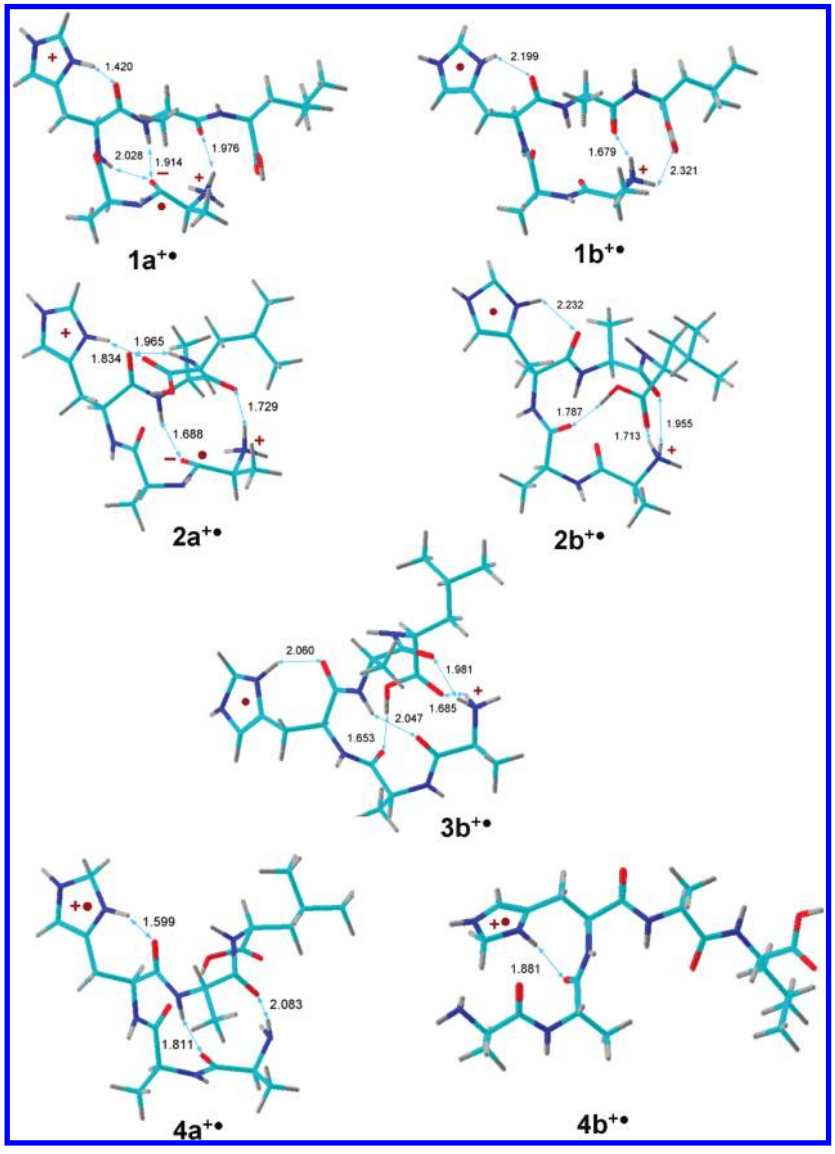

Figure 5. M06-2X/6-31+G(d,p) optimized structures of charge-reduced (AAHAL + 2H)$^{+\bullet}$. Structure description as in Figure 1 except that all hydrogen atoms are shown.

dx.doi.org/10.1021/jp3000784 | J. Phys. Chem. B 2012, 116, 3445−3456

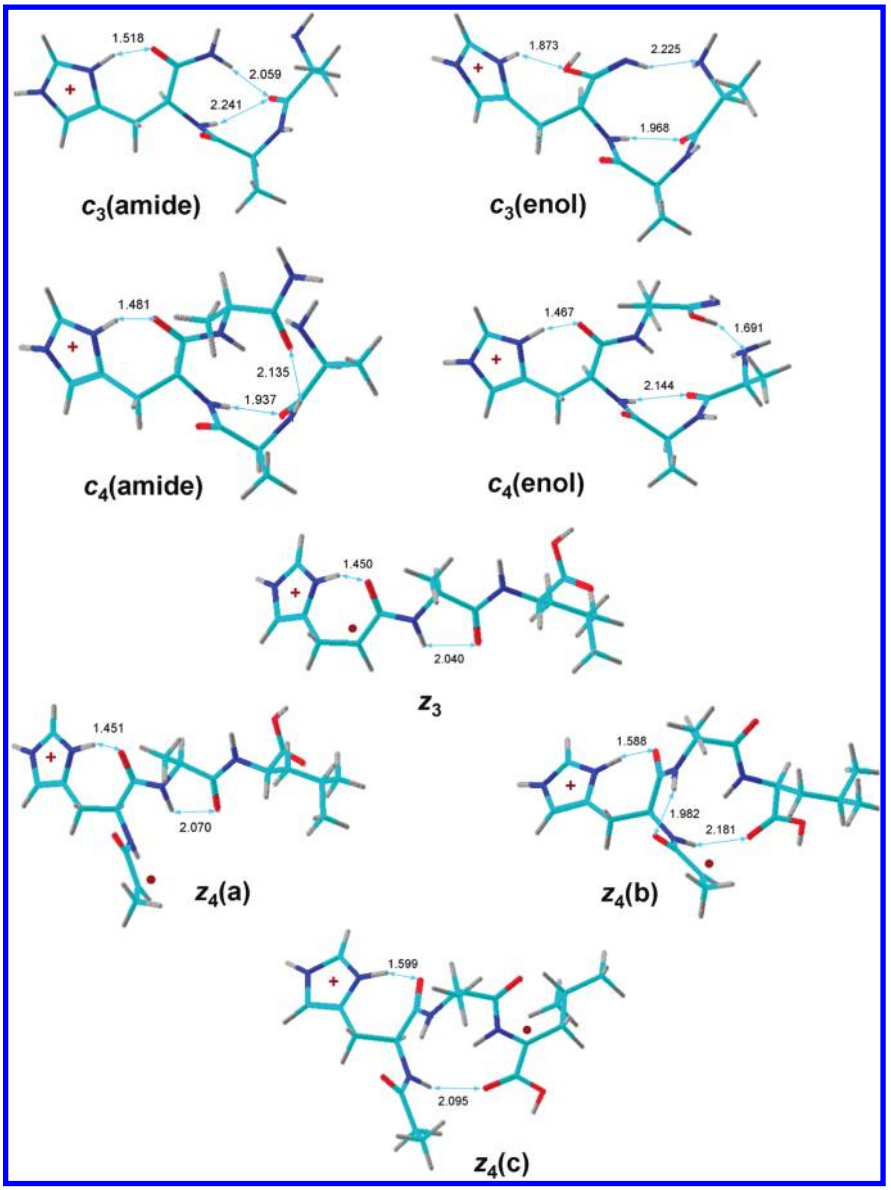

Figure 6. M06-2X/6-31+G(d,p) optimized structures of ETD *c* and *z* fragment ions. Structure description as in Figure 1 except that all hydrogen atoms are shown.

indicated that Coulomb repulsion between the charged groups in the dications was efficiently counter-balanced by internal solvation. Furthermore, we found that the very stable cation-radical $\mathbf{4b}^{+\bullet}$ did not match the experimental Ω and was likely absent in the population of charge-reduced species. A possible interpretation is that the formation of $\mathbf{4b}^{+\bullet}$ is kinetically controlled by charge-reduced ion refolding that is required to bring the ammonium group in $\mathbf{1b}^{+\bullet}$, $\mathbf{2b}^{+\bullet}$, or $\mathbf{3b}^{+\bullet}$ to the proximity of the His imidazole ring in order to facilitate exothermic proton transfer.[37] Regarding the distinction of $\mathbf{1a}^{+\bullet}$ and $\mathbf{1b}^{+\bullet}$, the previous study of the potential energy surface of zwitterion $\mathbf{1a}^{+\bullet}$ indicated that it was prone to a very facile dissociation by loss of ammonia in competition with proton migration forming an aminoketyl radical.[37] Hence, $\mathbf{1a}^{+\bullet}$ is likely to be depleted by these reactions on the time scale of the IM measurements. This leaves the histidine radical $\mathbf{1b}^{+\bullet}$ as a plausible candidate to be observed by ion mobility mass spectrometry.

It should be noted that, according to the calculations, the charge-reduced cation-radicals have quite distinct IR spectra that should allow them to be distinguished by ETD-IRMPD when instruments for this technique become available. For example (Figure S4, Supporting Information), the IR spectra of $\mathbf{1a}^{+\bullet}$ and $\mathbf{1b}^{+\bullet}$ show different frequencies for the carboxyl C═O stretching mode (1802 and 1766 cm^{-1}, respectively) and the Ala-4 C═O stretching mode (1698 and 1658 cm^{-1}, respectively). These differences are due to the different hydrogen bonding to the N-terminal ammonium group of the involved carbonyl groups, which is stronger in $\mathbf{1b}^{+\bullet}$ (Figure 5). The IR spectra of the cation-radicals also show a large difference in the bands for the imidazole C═C stretching mode, which for $\mathbf{1a}^{+\bullet}$ appears as a strong absorption band at 1612 cm^{-1} and is coupled to the His amide C═O stretching mode. In contrast, the analogous vibrational mode in $\mathbf{1b}^{+\bullet}$ appears as a weak band at 1661 cm^{-1}. The characteristics of the imidazole C═C frequency in $\mathbf{1a}^{+\bullet}$ are due to the conjugated

dx.doi.org/10.1021/jp3000784 | J. Phys. Chem. B 2012, 116, 3445−3456

nature of the planar imidazolium ring and a large change of the dipole moment upon the vibration of the charge-carrying ring.

ETD Fragment Ions. Ion mobility arrival times and the corresponding Ω were also determined for fragment ions c_3, c_4, z_3, and z_4 formed by ETD of $(AAHAL + 2H)^{2+}$ (Figure 4b) and compared to the Ω calculated for the optimized ion structures (Figure 6). The measured Ω showed a remarkably close agreement with those calculated for the c_3 and c_4 ion structures (Figure 6). The c ions were considered as both tautomeric forms, which were the enolimines presumably formed by ETD and their more stable amide tautomers. The c_3(amide) tautomer (Figure 6) was calculated to be 102 and 103 kJ mol^{-1} more stable than the c_3(enol) form by M06-2X and B3-MP2, respectively. Remarkably, the energy difference between the c_4(amide) and c_4(enol) was substantially smaller, $\Delta H_{g,0}$ = 49 and 57 kJ mol^{-1} by M06-2X and B3-MP2, respectively, again favoring the amide form. This effect can be due to the strong hydrogen bond between the enol imine hydroxyl and the N-terminal amino group in the c_4(enol) tautomer (Figure 6). The very similar Ω calculated for the enolimine and amide c_3 and c_4 tautomers are due to similar ion conformations, which are mainly determined by the internal solvation of the protonated His ring and the terminal enolimine or amide groups (Figure 6). At the same time, the similar Ω do not allow us to distinguish the enolimine and amide forms by ion mobility measurements. However, the enolimine and amide forms of the c_3 and, to a lesser extent, c_4 ions gave distinct theoretical IR spectra (Figure S5, Supporting Information), which indicated that the c ion tautomers possibly could be distinguished by IRMPD. Unfortunately, instruments for IRMPD spectra measurements of ETD fragments are currently unavailable to test the theoretical predictions.

Structure assignment of the z_3 and z_4 fragment ions was more complicated because of possible rearrangements by H atom migrations forming new tautomers with internal C_α radical sites.[79] The experimental Ω for the z_3 fragment showed a good match with the Ω calculated for the structure having the radical center at the terminal C_α position (Table 4). Among the z_4 fragment ions, the extended structure z_4(a) had a Ω that was 5−10% larger than the TWAVE experimental value. A closer match was obtained for rotamer z_4(b), having the radical center at the terminal C_α position, as formed initially by N−C_α bond cleavage, but also for an internal C_α radical z_4(c). It appears that ion mobility alone is unable to distinguish these radical tautomers on the basis of their very similar Ω. However, the above finding for $\mathbf{1b}^{+\bullet}$, $\mathbf{2b}^{+\bullet}$, and $\mathbf{3b}^{+\bullet}$ that post-ETD ion isomerizations were kinetically constrained can be extended by arguing that hydrogen−atom migrations in the z_3 and z_4 fragments were slow on the time scale of the ion mobility measurements, and therefore the z fragment ions were C_α terminal radicals. Previous analysis of z_4 ion dissociations indicated 100−132 kJ mol^{-1} energy barriers for H atom migrations between the terminal and Leu-C_α positions in z_4(a),[79] which is consistent with the assumption that the migration requires further activation and does not proceed in stable z_4 ions formed by ETD.

CONCLUSIONS

Structure analysis of gas-phase $(AAHAL + 2H)^{2+}$ ions utilizing ion mobility and IRMPD experiments in combination with multiple levels of theory allowed us to identify the conformer produced by electrospray ionization. TWAVE ion mobility measurements, complemented by multilevel electron structure calculations, allowed us to investigate the structures of charge-reduced peptide cation-radicals, as well as c and z fragment ions from electron transfer dissociation and to arrive at plausible structures for these species. We found, rather unexpectedly, that the charge-reduced peptide cation-radicals had collisional cross sections that were nearly identical to those of the precursor dications. This indicated that the peptide cation-radicals retained specific hydrogen bonding motifs from the precursor ion. A combination of multilevel theoretical calculations, including different density functional theory as well as perturbational methods, with experimental ion mobility methods is a powerful tool for structure assignment of precursor ions and electron transfer intermediates and fragments.

Table 4. Collisional Cross Sections of Charge-Reduced and ETD Fragment Ions

ion		cross section (Ω, Å^2)			
		PA[a]		TM (tuned He)[b]	
		B3LYP	M06-2X	B3LYP	M06-2X
$\mathbf{1a}^{+\bullet}$		157	150.4	156	148.3
$\mathbf{1b}^{+\bullet}$		156	151.8	156	150.9
$\mathbf{2a}^{+\bullet}$		146	141	149	143
$\mathbf{2b}^{+\bullet}$		148.6	145.7	149.5	146.0
$\mathbf{3b}^{+\bullet}$		148	145.2	150	147
$\mathbf{4a}^{+\bullet}$		150	145.7	151.1	146.7
$\mathbf{4b}^{+\bullet}$		159	158.6	160	155.7
exp. TWAVE		149			
c_3 (amide)		111	107.7	106	102.3
c_3 (enol)		109.1	107.6	104.9	103.4
exp. TWAVE		106.5			
c_4 (amide)		126	120.2	125.5	118.0
c_4 (enol)		123	117.5	121	118.5
exp. TWAVE		122			
z_3		128	126.1	121	119.6
exp. TWAVE		116			
z_4	(a)	145	142.7	140	138.1
	(b)	138	133.9	136	131.7
	(c)	138	130.7	135	128.1
exp. TWAVE		132			

[a]Calculations using the projection approximation method. [b]Calculations using the trajectory method.

ASSOCIATED CONTENT

Supporting Information

Figures S1−S5 and Tables S1−S40 of M06-2X/6-31+G(d,p) and B3LYP/6-31+G(d,p) optimized geometries in the Cartesian coordinate format. This material is available free of charge via the Internet at http://pubs.acs.org.

AUTHOR INFORMATION

Present Addresses

[⊥]Department of Molecular Structure, Amgen Inc., Thousand Oaks, CA, 91320

[#]National High Magnet Field Laboratory, Tallahassee, FL

Notes

The authors declare no competing financial interest.

ACKNOWLEDGMENTS

F.T. thanks the National Science Foundation (Grant CHE-1055132) for funding and Ecole Polytechnique Palaiseau for a

Visiting Professorship in September−October 2010. J.C.-R. and F.T. thank P. Maitre, J. M. Ortega, and J. P. Berthet for their support during the experiments at the CLIO facility.

REFERENCES

(1) Holmes, J. L. *Org. Mass Spectrom.* **1985**, *20*, 169−183.
(2) Dunbar, R. C. *Int. J. Mass Spectrom.* **2000**, *200*, 571−589.
(3) Rizzo, T. R.; Stearns, J. A.; Boyarkin, O. V. *Int. Rev. Phys. Chem.* **2009**, *28*, 481−515.
(4) Baer, T.; Dunbar, R. C. *J. Am. Soc. Mass Spectrom.* **2010**, *21*, 681−693.
(5) Prazeres, R.; Glotin, F.; Insa, C.; Jaroszynski, D. A.; Ortega, J. M. *Eur. Phys. J. D* **1998**, *3*, 87−93.
(6) Valle, J. J.; Eyler, J. R.; Oomens, J.; Moore, D. T.; van der Meer, A. F. G.; von Helden, G.; Meijer, G.; Hendrickson, C. L.; Marshall, A. G.; Blackney, G. T. *Rev. Sci. Instrum.* **2005**, *76*, 023103−1−023103−7.
(7) Jarrold, M. F. *Acc. Chem. Res.* **1999**, *32*, 360−367.
(8) Hudgins, R. R.; Mao, Y.; Ratner, M. A.; Jarrold, M. F. *Biophys. J.* **1999**, *76*, 1591−1597.
(9) Hudgins, R. R.; Jarrold, M. F. *J. Am. Chem. Soc.* **1999**, *121*, 3494−3501.
(10) Kinnear, B. S.; Hartings, M. R.; Jarrold, M. F. *J. Am. Chem. Soc.* **2001**, *123*, 5660−5667.
(11) Prell, J. S.; O'Brien, J. T.; Williams, E. R. *J. Am. Soc. Mass Spectrom.* **2010**, *21*, 800−809.
(12) Polfer, N. C.; Paizs, B.; Snoek, L. C.; Compagnon, I.; Suhai, S.; Meijer, G.; von Helden, G.; Oomens., J. *J. Am. Chem. Soc.* **2005**, *127*, 8571−8579.
(13) Prell, J. S.; Demireva, M.; Jos Oomens, J.; Williams, E. R. *J. Am. Chem. Soc.* **2009**, *131*, 1232−1242.
(14) Dunbar, R. C.; Steill, J. D.; Polfer, N. C.; Oomens, J. *J. Phys. Chem. B* **2009**, *113*, 10552−10554.
(15) Engelhart, A. E.; Morton, T. H.; Hud, N. V. *Chem. Commun.* **2009**, 647−649.
(16) Oomens, J.; Moehlig, A. R.; Morton, T. H. *J. Phys. Chem. Lett.* **2010**, *1*, 2891−2897.
(17) Shvartsburg, A. A.; Mashkevich, S. V.; Baker, E. S.; Smith, R. D. *J. Phys. Chem. A* **2007**, *111*, 2002−2010.
(18) Shvartsburg, Siu, M. K. W.; A., A.; Clemmer, D. E. *J. Am. Soc. Mass Spectrom.* **2001**, *12*, 885−888.
(19) Shvartsburg, A. A.; Smith, R. D. *Anal. Chem.* **2008**, *80*, 9689−9699.
(20) Vosko, S. H.; Wilk, L.; Nusair, M. *Can. J. Phys.* **1980**, *58*, 1200−1211.
(21) Lee, C.; Yang, W.; Parr, R. G. *Phys. Rev. B: Condensed Matter Mater. Phys.* **1988**, *37*, 785−789.
(22) Vydrov, O. A.; Scuseria, G. E. *J. Chem. Phys.* **2004**, *121*, 8187−8193.
(23) Haunschild, R.; Henderson, T. M.; Jimenez-Hoyos, C. A.; Scuseria, G. E. *J. Chem. Phys.* **2010**, *133*, 134116/1−134116/10.
(24) Perdew, J. P.; Ruzsinszky, A. *Int. J. Quantum Chem.* **2010**, *110*, 2801−2807.
(25) Moss, C. L.; Chung, T. W.; Čeřovský, V.; Tureček, F. *Collect. Czech. Chem. Commun.* **2011**, *76*, 295−309.
(26) Tureček, F. *J. Phys. Chem. A* **1998**, *102*, 4703−4713.
(27) Wu, R.; McMahon, T. B. *J. Phys. Chem. B* **2009**, *113*, 8767−8775.
(28) Dunbar, R. C.; Steill, J. D.; Polfer, N. C.; Oomens, J. *Int. J. Mass Spectrom.* **2009**, *283*, 77−84.
(29) Wu, R.; McMahon, T. B. *ChemPhysChem* **2008**, *9*, 2826−2835.
(30) Wu, R.; McMahon, T. B. *Chem.—Eur. J.* **2008**, *14*, 7765−7770.
(31) Wu, R.; McMahon, T. B. *J. Am. Chem. Soc.* **2007**, *129*, 11312−11313.
(32) Correia, C. F.; Clavaguera, C.; Erlekam, U.; Scuderi, D.; Ohanessian, G. *ChemPhysChem* **2008**, *9*, 2564−2573.
(33) Correia, C. F.; Balaj, P. O.; Scuderi, D.; Maitre, P.; Ohanessian, G. *J. Am. Chem. Soc.* **2008**, *130*, 3359−3370.
(34) Yanai, T.; Tew, D. P.; Handy, N. C. *Chem. Phys. Lett.* **2004**, *393*, 51−57.
(35) Zhao, Y.; Truhlar, D. G. *Theor. Chem. Acc.* **2008**, *120*, 215−241.
(36) Gilson, T. W.; van der Rest, G.; Chamot-Rooke, J.; Kurlancheek, W.; Head-Gordon, M.; Jacquenin, D.; Frison, G. *J. Phys. Chem. Lett.* **2011**, *2*, 1426−1431.
(37) Tureček, F.; Chung, T. W.; Moss, C. L.; Wyer, J. A.; Ehlerding, A.; Holm, A. I. S.; Zettergren, H.; Nielsen, S. B.; Hvelplund, P.; Chamot-Rooke, J.; Bythell, B.; Paizs, B. *J. Am. Chem. Soc.* **2010**, *132*, 10728−10740.
(38) Turecek, F.; Jones, J. W.; Towle, T.; Panja, S.; Nielsen, S. B.; Hvelplund, P.; Paizs, B. *J. Am. Chem. Soc.* **2008**, *130*, 14584−14596.
(39) Tureček, F.; Yao, C.; Fung, Y. M. E.; Hayakawa, S.; Hashimoto, M.; Matsubara, H. *J. Phys. Chem. B* **2009**, *113*, 7347−7366.
(40) Chung, T. W.; Turecek, F. *Int. J. Mass Spectrom.* **2011**, *306*, 99−107.
(41) Lemaire, J.; Boissel, P.; Heninger, M.; Mauclaire, G.; Bellec, G.; Mestdagh, H.; Simon, A.; Caer, S. L.; Ortega, J. M.; Glotin, F.; Maitre, P. *Phys. Rev. Lett.* **2002**, *89*, 273002−273004.
(42) Bush, M. F.; Hall, Z.; Giles, K.; Hoyes, J.; Robinson, C. V.; Ruotolo, B. T. *Anal. Chem.* **2010**, *82*, 9557−9565.
(43) Mason, E. A.; McDaniel, E. W. *Transport properties of ions in gases*; Wiley: New York, 1998; pp 149, 408.
(44) Pringle, S. D.; Giles, K.; Wildgoose, J. L.; Williams, J. P.; Slade, S. E.; Bateman, R. H.; Bowers, M. T.; Scrivens, J. H. *Int. J. Mass Spectrom.* **2007**, *261*, 1−10.
(45) Giles, K.; Wildgoose, J. L.; Langridge, D. J.; Campuzano, I. *Int. J. Mass Spectrom.* **2010**, *298*, 10−16.
(46) Giles, K.; Williams, J. P.; Campuzano, I. *Rapid Commun. Mass Spectrom.* **2011**, *25*, 1559−1566.
(47) http://www.indiana.edu/~clemmer/Research/cross%20section%20database/Peptides/polyaminoacid_cs.htm)
(48) Kemper, P. R.; Dupuis, N. F.; Bowers, M. T. *Int. J. Mass Spectrom.* **2009**, *287*, 46−57.
(49) Paizs, B.; Suhai, S.; Hargittai, B.; Hruby, V. J.; Somogyi, A. *Int. J. Mass Spectrom.* **2002**, *219*, 203−232.
(50) Case, D. A.; Pearlman, D. A.; Caldwell, J. W.; Cheatham, T. E., III; Ross, W. S.; Simmerling, C. L.; Darden, T. A.; Merz, K., M.; Stanton, R. V.; Cheng, A. L.; Vincent, J. J.; Crowley, M.; Tsui, V.; Radmer, R. J.; Duan, Y.; Pitera, J.; Massova, I. G.; Seibel, G. L.; Singh, U. C.; Weiner, P. K.; Kollmann, P. A. In; *AMBER 99*, University of California: San Francisco, 1999.
(51) Frisch, M. J.; Trucks, G. W.; Schlegel, H. B.; Scuseria, G. E.; Robb, M. A.;Cheeseman, J. R.; Montgomery, J. A., Jr.; Vreven, T.; Kudin, K. N.; Burant, J. C.; Millam, J. M.; Iyengar, S. S.; Tomasi, J.; Barone, V.; Mennucci, B.; Cossi, M.; Scalmani, G.; Rega, N.; Petersson, G. A.; Nakatsuji, H.; Hada, M.; Ehara, M.; Toyota, K.; Fukuda, R.; Hasegawa, J.; Ishida, M.; Nakajima, T.; Honda, Y.; Kitao, O.; Nakai, H.; Klene, M.; Li, X.; Knox, J. E.; Hratchian, H. P.; Cross, J. B.; Adamo, C.; Jaramillo, J.; Gomperts, R.; Stratmann, R. E.; Yazyev, O.; Austn, A. J.; Cammi, R.; Pomelli, C.; Ochterski, J., W.; Ayala, P. Y.; Morokuma, K.; Voth, G. A.; Salvador, P.; Dannenberg, J. J.; Zakrzewski, V. G.; Dapprich, S.; Daniels, A. D.; Strain, M. C.; Farkas, O.; Malick, D. K.; Rabuck, A. D.; Raghavachari, K.; Foresman, J. B.; Ortiz, J. V.; Cui, Q.; Baboul, A. G.; Clifford, S.; Cioslowski, J.; Stefanov, B. B.; Liu, G.; Liashenko, A.; Piskorz, P.; Komaromi, I.; Martin, R. L.; Fox, D. J.; Keith, T.; Al-Laham, M. A.; Peng, C. Y.; Nanayakkara, A.; Challacombe, M.; Gill, P. M. W.; Johnson, B.; Chen, W.; Wong, M. W.; Gonzalez, C.; Pople, J. A. *Gaussian 03, Revision B.05*; Gaussian, Inc.; Pittsburgh PA, 2003.
(52) Moss, C. L.; Chung, T. W.; Wyer, J. A.; Nielsen, S. B.; Hvelplund, P.; Tureček, F. *J. Am. Soc. Mass Spectrom.* **2011**, *22*, 731−751.
(53) Phillips, J. C.; Braun, R.; Wang, W.; Gumbart, J.; Tajkhorshid, E.; Villa, E.; Chipot, C.; Skeel, R. D.; Kale, L.; Schulten, K. *J. Comput. Chem.* **2005**, *26*, 1781−1802.
(54) MacKerell, A. D. Jr.; Bashford, D.; Bellott, M.; Dunbrack, R. L. Jr.; Evanseck, J. D.; Field, M. J.; Fischer, S.; Gao, J.; Guo, H.; Ha, S.; Joseph-McCarthy, D.; Kuchnir, L.; Kuczera, K.; Lau, F. T. K.; Mattos,

C.; Michnick, S.; Ngo, T.; Nguyen, D. T.; Prodhom, B.; Reiher, W. E. III; Roux, B.; Schlenkrich, M.; Smith, J. C.; Stote, R.; Straub, J.; Watanabe, M.; Wiorkiewicz-Kuczera, J.; Yin, D.; Karplus, M. *J. Phys. Chem. B* **1998**, *102*, 3586−3616.
(55) Sugita, Y.; Okamoto, Y. *Chem. Phys. Lett.* **1999**, *314*, 141−151.
(56) Stewart, J. J. P. *J. Mol. Model.* **2007**, *13*, 1173−1213.
(57) Becke, A. D. *J. Chem. Phys.* **1993**, *98*, 1372−1377.
(58) Becke, A. D. *J. Chem. Phys.* **1993**, *98*, 5648−5652.
(59) Stephens, P. J.; Devlin, F. J.; Chabalowski, C. F.; Frisch, M. J. *J. Phys. Chem.* **1994**, *98*, 11623−11627.
(60) Chai, J.-D.; Head-Gordon, M. *J. Chem. Phys.* **2008**, *128*, 084106/1−15.
(61) Møller, C.; Plesset, M. S. *Phys. Rev.* **1934**, *46*, 618−622.
(62) Frisch, M. J.; Trucks, G. W.; Schlegel, H. B.; Scuseria, G. E.; Robb, M. A.; Cheeseman, J. R.; Scalmani, G.; Barone, V.; Mennucci, B.; Petersson, G. A.; Nakatsuji, H.; Caricato, M.; Li, X.; Hratchian, H. P.; Izmaylov, A. F.; Bloino, J.; Zheng, G.; Sonnenberg, J. L.; Hada, M.; Ehara, M.; Toyota, K.; Fukuda, R.; Hasegawa, J.; Ishida, M.; Nakajima, T.; Honda, Y.; Kitao, O.; Nakai, H.; Vreven, T.; Montgomery, J. A., Jr.; Peralta, J. E.; Ogliaro, F.; Bearpark, M.; Heyd, J. J.; Brothers, E.; Kudin, K. N.; Staroverov, V. N.; Kobayashi, R.; Normand, J.; Raghavachari, K.; Rendell, A.; Burant, J. C.; Iyengar, S. S.; Tomasi, J.; Cossi, M.; Rega, N.; Millam, J. M.; Klene, M.; Knox, J. E.; Cross, J. B.; Bakken, V.; Adamo, C.; Jaramillo, J. ; Gomperts, R.; Stratmann, R. E. ; Yazyev, O.; Austin, A. J. ;Cammi, R.; Pomelli, C.; Ochterski, J. W.; Martin, R. L.; Morokuma, K.; Zakrzewski, V. G.; Voth, G. A.; Salvador, P.; Dannenberg, J. J.; Dapprich, S.; Daniels, A. D.; Farkas, O.; Foresman, J. B.; Ortiz, J. V. ; Cioslowski, J.; Fox, D. J.; *Gaussian 09, Revision A.02;* Gaussian, Inc.; Wallingford CT, 2009.
(63) http://www.indiana.edu/~nano/software.html.
(64) von Helden, G.; Hsu, M.-T.; Gotts, N.; Bowers, M. T. *J. Phys. Chem.* **1993**, *97*, 8182−8192.
(65) Bleiholder, C.; Wyttenbach, T.; Bowers, M. T. *Int. J. Mass Spectrom.* **2011**, *308*, 1−10.
(66) Mesleh, M. F.; Hunter, J. M.; Shvartsburg, A. A.; Schatz, G. C.; Jarrold, M. F. *J. Phys. Chem.* **1996**, *100*, 16082−16086.
(67) Reed, A. E.; Weinstock, R. B.; Weinhold, F. *J. Chem. Phys.* **1985**, *83*, 735−746.
(68) Campuzano, I.; Bush, M. F.; Robinson, C. V.; Beaumont, C.; Richardson, K.; Kim, H.; Kim, H. I. *Anal. Chem.* **2012**, DOI: 10.1021/ac202625t.
(69) Knapman, T. W.; Berryman, J. T.; Campuzano, I.; Harris, S. A.; Ashcroft, A. E. *Int. J. Mass Spectrom.* **2010**, *298*, 17−23.
(70) Yamazaki, T. Y.; Sato, H.; Hirata, F. *J. Chem. Phys.* **2003**, *119*, 6663−6670.
(71) Niedermeyer, H.; Ab Rani, M. A.; Lickiss, P. D.; Hallett, J. P.; Welton, T.; White, A. J. P.; Hunt, P. A. *Phys. Chem. Chem. Phys.* **2010**, *12*, 2018−2029.
(72) Foresman, J. B.; Frisch., A. E. *Exploring Chemistry with Electronic Structure Methods*, 2nd ed.; Gaussian, Inc.: Pittsburgh, PA, 1996; p 115.
(73) Rassolov, V. A.; Ratner, M. A.; Pople, J. A. *J. Chem. Phys.* **2000**, *112*, 4014−4019.
(74) Perticolas, W. L. *Methods Enzymol.* **1979**, *61*, 425−458.
(75) Frison, G.; Bull, A.; van der Rest, G.; Tureček, F.; Besson, T.; Lemaire, J.; Maître, P.; Chamot-Rooke, J. *J. Am. Chem. Soc.* **2008**, *130*, 14916−14917.
(76) Rand, K. D.; Pringle, S. D.; Morris, M.; Engen, J. R.; Brown, J. M. *J. Am. Soc, Mass Spectrom.* **2011**, *22*, 11784−1793.
(77) Nguyen, V. Q.; Turecek, F. *J. Mass Spectrom.* **1996**, *31*, 1173−1184.
(78) Chung, T. W.; Tureček, F. *Int. J. Mass Spectrom.* **2011**, *301*, 55−61.
(79) Chung, T. W.; Tureček, F. *J. Am. Soc. Mass Spectrom.* **2010**, *21*, 1279−1295.